Thresholds for post-rebound SHIV control after CCR5 gene-edited autologous hematopoietic cell transplantation

Short title: SHIV remission after ΔCCR5 HSPC transplantation

E. Fabian Cardozo[1], Elizabeth R. Duke[1,3], Christopher W. Peterson[2,3], Daniel B. Reeves[1], Bryan T Mayer[1], Hans-Peter Kiem[2,3,4], Joshua T. Schiffer[1,2,3,*]

[1]Vaccine and Infectious Disease Division,

[2]Clinical Research Division, Fred Hutchinson Cancer Research Center, Seattle, WA, USA;

[3]Department of Medicine and

[4]Department of Pathology, University of Washington, Seattle, WA, USA.

*Corresponding Author. Address: 1100 Fairview Ave. N. MS E4-100, Seattle, WA, 98119;

email: jschiffe@fredhutch.org; phone: (206)667-7359.

Text word count: 3896.

Abstract word count: 246.

Number of figures: 7.

Number of tables: 1.

Key Points

- Data-validated modeling suggest that loss of immune response after transplantation produces more depletion of $CD4^{+}CCR5^{+}$ T cells post-ATI.
- The minimum fraction of transplanted gene-edited cells for viral control linearly relates with the $CD4^{+}CCR5^{+}$ T cell nadir 10 weeks post-ATI.

Abstract (246/250 words)

The two recent cases of HIV cure/stable remission following allogeneic stem cell transplantation are difficult to reproduce because of the toxicity of the procedure and rarity of donors homozygous for the CCR5Δ32 deletion. One approach to overcome these barriers is the use of autologous, CCR5 gene-edited hematopoietic stem and progenitor cell (HSPC) products. Unlike allogeneic transplantation, in which the frequency of CCR5Δ32 donor cells approaches 100%, the CCR5 gene can currently only be edited *ex vivo* in a fraction of autologous HSPCs. Therefore, we sought to determine the minimum fraction required for viral control using mathematical modeling. We analyzed data from eight juvenile pigtail macaques infected intravenously with SHIV-1157ipd3N4, treated with combination antiretroviral therapy (cART), and infused with autologous HSPCs without CCR5 gene editing. We developed a mathematical model that simultaneously describes reconstitution of $CD4^+CCR5^+$, $CD4^+CCR5^-$, and $CD8^+$ T cell counts, as well as SHIV plasma viral loads in control and transplanted macaques. The model predicts that transplantation decreases the immunologic response to SHIV to varying degrees in macaques. By modifying the model to hypothetically describe transplantation with a given fraction of protected CCR5-edited cells we found that loss of immunologic response correlated with a more profound depletion of $CCR5^+CD4^+$ T cells and a higher fractions of gene-edited cells required for cART-free viral remission. Our results provide a framework to predict the likelihood of post-rebound control *in vivo* using the percentage of CCR5-edited cells in peripheral blood and the loss of HIV-specific immunity following autologous HSPC.

(Main text: 3896/4000 words, including headings)

INTRODUCTION

The major obstacle to HIV-1 eradication is a latent reservoir of long-lived infected cells[1-3]. Cure strategies aim to eliminate all infected cells or permanently prevent viral reactivation from latency. The only known case of HIV cure[4,5] and an additional, recently-reported case of prolonged remission[6], resulted from allogeneic hematopoietic stem cell transplant with homozygous CCR5Δ32 donor cells[4-6]. The success of this procedure is likely multifactorial—in part attributable to HIV resistance of the transplant product, the conditioning regimen that facilitates engraftment and also eliminates infected cells, graft-versus-host effect, and immunosuppressive therapies for graft-versus-host disease[7-11].

A current research focus is to recapitulate this method of cure with minimal toxicity. One method is to perform autologous transplantation following *ex vivo* inactivation of the CCR5 gene with gene editing nucleases, eliminating the need for allogeneic CCR5-negative donors[12,13]. While this procedure is safe and feasible in pigtail macaques infected with simian-human immunodeficiency virus (SHIV)[13-16], only a fraction of HSPCs can be genetically modified *ex vivo* to be HIV-resistant.

To address this challenge, we developed a mathematical model to predict the minimum threshold of persisting, gene-modified cells necessary for functional cure. First, we modeled the kinetics of $CD4^+CCR5^+$, $CD4^+$ $CCR5^-$, and $CD8^+$ T cell reconstitution after autologous transplantation. We then modeled SHIV rebound kinetics following analytical treatment interruption (ATI) and identified the degree of loss of anti-HIV cytolytic immunity following transplantation. Finally, we projected the proportion of gene-modified cells and the levels of SHIV-specific immunity required to eliminate viral replication following ATI.

METHODS

Experimental Data

Eight juvenile pigtail macaques were intravenously challenged with 9500 TCID50 SHIV-1157ipd3N4 (SHIV-C)[14,17]. After 6 months, the macaques received combination antiretroviral therapy (cART: tenofovir [PMPA], emtricitabine [FTC], and raltegravir [RAL]). After ~30 weeks on cART, four animals received total body irradiation (TBI) followed by transplantation of autologous HSPCs. After an additional 25 weeks following transplant, when viral load was fully suppressed, animals underwent analytical treatment interruption (ATI) of cART[14]. A control group of four animals did not receive TBI or HSPC transplantation and underwent ATI after ~50 weeks of treatment (**Fig. 1A**). Plasma viral loads and absolute quantified $CD4^+CCR5^-$, $CD4^+CCR5^+$ and $CD8^+$ total and subsets (naïve, central memory [T_{CM}], and effector memory [T_{EM}]) T cell counts from peripheral blood were measured as described previously[14,17]. We analyzed peripheral T cell counts and plasma viral load from transplant until 43 weeks post-transplant (~25 weeks pre-ATI and ~20 weeks post-ATI).

Mathematical modeling

We employed several series of ordinary differential equation models of cellular and viral dynamics after transplantation (**Fig. 1B**). First, we modeled T cell dynamics and reconstitution following transplant and before ATI, assuming that low viral loads on ART do not affect cell dynamics (**Fig. 1C**). After curation of that model, we introduced viral dynamics and fit those to the T cell and viral rebound dynamics from the animals pre- and post-ATI (**Fig. 1D**). Lastly, we applied our complete model to a transplant scenario with gene editing of CCR5 to predict the minimal threshold of editing for functional HIV cure (**Fig. 1E**).

T cell reconstitution after transplantation: We modeled the kinetics of $CD4^+$ and $CD8^+$ T cell subsets in blood, transplanted cells that home to the BM, and progenitor cells in the BM/thymus as shown in **Fig. 1C**. We included $CD8^+$ T cells in the model because $CD8^+$ and $CD4^+$ T cells may arise from new naïve cells from the thymus and compete for resources that impact clonal expansion and cell survival[18-20]. At the moment of HSPC infusion, transplanted animals are lymphopenic due to TBI. The control group did not have a transplanted-cell compartment, and all other compartments remained in steady state. We assumed that $CD4^+$ and $CD8^+$ T cell expansion may have two possible drivers: (1) lymphopenia-induced proliferation of mature cells that persist through myeloablative TBI[18,21-25], and (2) differentiation from naïve cells from progenitors in the thymus (from transplanted $CD34^+$ HSPCs[26,27] or $CD34^+$ HSPCs that persist following TBI) and further differentiation to an activated effector state[24,25,28-32]. We assumed that in a lymphopenic environment, factors that drive T cell proliferation are more accessible (i.e., self-MHC molecules on antigen-presenting cells[28,29,33,34] and γ-chain cytokines such as IL-7 and IL-15[21-23,35-37]). However, as they grow, cells compete for access to these resources, limiting clonal expansion[18] such that logistic growth models are appropriate[19]. We assume that new peripheral $CD4^+$ and $CD8^+$ T naïve cells come from a progenitor compartment in the BM/Thymus[38,39]. For $CD4^+$ T cells, we assume that naïve cells do not express CCR5[40-42], and subsequently up- and/or down-regulate expression of the CCR5 receptor[30]. For $CD8^+$ T cells, we included a single $CD8^+$ memory precursor compartment of T_N and T_{CM} cells that differentiate linearly into T_{EM} during lymphopenia[43-45]. The details of the model are presented in the **Supp. Material** and in **Fig. 1C** with the notation described in **Table 1**. A parsimonious, curated version

of this model was selected from a series of models with varying mechanistic and statistical complexity as presented in the **Supp. Materials.**

T cell and viral dynamics: We next adapted the curated T cell reconstitution model by combining several adaptations of the canonical model of viral dynamics[43-53] as shown in **Fig. 1D**. The model assumes that SHIV infects only $CD4^+CCR5^+$ T cells[17] and that a small fraction (~ 5%) of those infected cells are able to produce infectious virus[51,54,55]. We modeled cART by reducing the infection rate to zero and modeled ATI by assuming infection is greater than zero after some time Δ_t after interruption. This model assumes that productively infected cells arise also from activation of a steady set of latently infected cells. The presence of both unproductively and productively infected cells leads to the expansion of $CD8^+$ $T_{naïve}$ and T_{CM} cells, from which the majority of dividing cells differentiate into SHIV-specific effector cells[30,46,47,52,53]. The details of the model are presented in the **Supp. Material** and in **Fig. 1D** with the notation described in **Table 1**. A parsimonious version of this model was selected from a series of models with varying mechanistic and statistical complexity as presented in the **Supp. Materials.**

Viral and T cell dynamics in the setting of ΔCCR5 HSPC transplantation: We next adapted our full model to simulate scenarios in which autologous transplantation includes cells that are CCR5-edited (**Fig 1E**). We added variables representing CCR5-edited HSPCs in different compartments: (1) infused HSPCs in blood, (2) T cell progenitors in BM/thymus, and (3) $CD4^+CCR5^-$ T cells in blood. These compartments have the same structure as CCR5-non-edited cells but with two differences. First, the value of gene-edited HSPCs at transplantation is a

fraction f_p of the total number of infused cells. Second, mature, CCR5-edited $CD4^+CCR5^-$ cells do not upregulate CCR5 (see full model in **Supp. Materials**).

Fitting procedure and model selection

To fit our models (**Fig. 1C-D**) to the transplant data, we used a nonlinear mixed-effects modeling approach[56] described in detail in the **Supp. materials**. Briefly, we estimated the population mean and variance for each model parameter using the Stochastic Approximation Expectation Maximization (SAEM) algorithm embedded in the Monolix software (www.lixoft.eu). For a subset of parameters, random effects were specified, and those variances were estimated. Measurement error variance was also estimated assuming an additive error model for the logged outcome variables.

We first fit instances of models with varying statistical and parameter complexity in **Fig. 1C** to blood T cell counts during transplant and before ATI assuming that one or multiple mechanisms are absent, or that certain mechanisms have equal kinetics (**Table S1** includes all 19 competing models). Then, we fit several instances of the model **Fig. 1D** to blood T cell counts and plasma viral load during the period after transplant including ATI using the best competing model (solid lines) for the model in **Fig. 1C** (**Table S2** includes all 15 competing models including viral dynamics). To determine the best and most parsimonious model among the instances, we computed the log-likelihood (log L) and the Akaike Information Criteria (AIC=-2log L+2m, where m is the number of parameters estimated)[57]. We assumed a model has similar support from the data if the difference between its AIC and the best model (lowest) AIC is less than two[57] (see **Supp. materials** for details).

Simulations for each animal were computed using individual-level parameter estimates generated from the predicted random effects of the fitted population model.

Data sharing statement. Original data will be shared upon request.

RESULTS

$CD4^+CCR5^+$ and $CD8^+$ T cells recover more rapidly than $CD4^+CCR5^-$ T cells after HSPC transplantation. We analyzed the kinetics of peripheral blood $CD4^+CCR5^+$ and $CD4^+CCR5^-$ T-cells, and total, $T_{naïve}$, T_{CM}, and T_{EM} $CD8^+$ T-cells in macaques after HSPC transplantation. In controls, levels of $CD4^+$ and $CD8^+$ T cells oscillated around a persistent set point (**Fig. S1**). $CD4^+CCR5^+$ T cell levels were ~100 cells/μl and were uniformly lower than the $CD4^+CCR5^-$ T cell counts (~1200 cells/μl) ($p=0.01$, paired t-test of the averaged post-transplant measures, **Fig. 2A**). Total $CD8^+$ T cell levels in the control group were ~1400 cells/μl with a greater contribution from T_{EM} (73%) than T_N+T_{CM} (27%) (based on median values, **Fig. 2B**).

In the transplant group, $CD4^+$ and $CD8^+$ T cells expanded at different rates from the remaining levels post-TBI (**Fig. 2C-D**). The levels of $CD4^+CCR5^+$ T cells started at 1-10 cells/μl and reconstituted to levels similar to the control group over 5-10 weeks (**Fig. 2D**). After TBI, $CD4^+CCR5^-$ T cells remained at higher levels (~100 cells/μl) than $CD4^+CCR5^+$ T cells but expanded more slowly and did not reach the values of the control group after 25 weeks (**Figs. 2C-D**). The $CD4^+CCR5^+$ T cell compartment expanded 8-fold more rapidly than the $CD4^+CCR5^-$ compartment ($p=0.01$, paired t-test, **Figs. 2C-D**). $CD8^+$ T cells decreased to levels between 10 and 100 cells/μl after TBI but recovered to levels below the control group in 5 weeks (**Figs. 2C-D**); $CD8^+$ T cells recovered as rapidly as the $CD4^+CCR5^+$ population (**Figs. 2C-D**).

Overall, these results show that after transplantation there is a faster reconstitution of $CD4^+CCR5^+$ and $CD8^+$ T cells compared to $CD4^+CCR5^-$ cells, suggesting each cell subset may have different mechanisms that drive their expansion. To explore these mechanisms, we analyzed the data in the context of mechanistic mathematical models of cell dynamics.

Lymphopenia-induced proliferation drives early $CD4^+CCR5^+$ and $CD8^+$ T cell reconstitution after HPSC transplantation. To identify the main drivers of T cell reconstitution after transplant, we developed a mathematical model that considered plausible mechanisms underlying reconstitution of distinct T cell subsets following autologous transplantation (**Fig. 1C**). We built 19 versions of the model by assuming that one or multiple mechanisms are absent, or by assuming certain mechanisms have equivalent or differing kinetics (**Table S1**). Using model selection theory based on AIC, we identified the model in **Fig. 1C** without the dashed lines which most parsimoniously reproduces the data (**Table S1**). The best fits of this model are presented in **Fig. 2D** and **Fig. S1** with the respective parameter estimates in **Tables S3-S4**. The main features of this model are: (1) $CD4^+CCR5^+$ T cell reconstitution after transplant is driven by proliferation and upregulation of CCR5; (2) $CD4^+CCR5^-$ T cell expansion is driven only by new naïve cells from the thymus and not proliferation; and (3), thymic export rates are equal between $CD4^+$ and $CD8^+$ naïve T cells.

The best fit model predicts that $CD4^+CCR5^-$ T cells have a delayed reconstitution that occurs only when cells from the thymus (estimated with rate ~0.01/day) outnumber their loss due to death, trafficking to tissues, or upregulation of CCR5. Furthermore, the estimated $CD4^+CCR5^+$ T cell proliferation rate (~0.1/day) far exceeds the estimated CCR5 upregulation (~0.004/day) and thymic export rates (~0.01/day). Therefore, one month after transplantation, the

total concentration of $CD4^+CCR5^+$ T new cells generated by proliferation is predicted to be 40-fold higher than the concentration generated by up-regulation of CCR5 (**Fig. 3**).

Our model predicts that $CD8^+$ T cells follow a similar pattern to $CD4^+CCR5^+$ T cells (**Fig. 2D**), as the $CD8^+$ T_{EM} proliferation rate is up to 10-fold higher than the $CD8^+$ T cell differentiation rate (**Fig. S2**). Overall, these results suggest that following autologous HSPC transplant: (1) slow thymic export is the main driver of $CD4^+CCR5^-$ T cell growth, and (2) rapid lymphopenia-induced proliferation of remaining cells (rather than transplanted cells) after TBI is the main driver for $CD4^+CCR5^+$ and $CD8^+$ T cell expansion.

Reduction of blood $CD4^+CCR5^+$ T cell counts correlates with plasma viral rebound after ATI in animals that underwent HSPC transplantation. We next aimed to extend previous analysis comparing plasma viral load rebound kinetics to $CD4^+CCR5^+$ and $CCR5^-$ T cell subset dynamics after ATI[14,51]. **Fig. 4** and **Fig. S3** presents the plasma viral loads and the blood $CD4^+CCR5^+$ and $CD4^+CCR5^-$ T cell kinetics before and after ATI in transplanted and control macaques respectively. Viral burden after ATI was more pronounced in the transplant group compared to the control group: median peak viral load was 10-fold higher (p=0.06, Mann-Whitney test. See **Fig. 4A**) and median final viral load measurements at necropsy were 2-$\log_{10}$ higher (p=0.06, Mann-Whitney test. See **Fig.4B**). $CD4^+CCR5^+$ T-cell counts decreased after ATI in the transplant group reaching a significantly lower nadir (~8-fold) than the control animals (p=0.01, Mann-Whitney test. **Fig. 4C**). The two animals with the largest reduction of $CD4^+CCR5^+$ T cells had the highest viral set points. There was no difference between control and transplant groups' $CD4^+CCR5^-$ T cell nadir: both groups had an average reduction of ~200 cells/μL (**Fig.4D**).

In the control group, individual plasma viral loads did not correlate with corresponding $CD4^+CCR5^+$ T-cell counts post-ATI. However, in three animals in the transplant group, viral load observations post-ATI correlated negatively with their corresponding $CD4^+CCR5^+$ T cell counts (**Fig. S4**).

Overall, these results show that transplanted animals had higher viral load that correlated with the reduction of $CD4^+CCR5^+$ T cells after ATI. This suggests that transplantation might affect macaques' immunologic response to SHIV so that the presence of the virus leads to more depletion of $CD4^+CCR5^+$ T cells. We explore this possibility by simultaneously analyzing the viral and T cell subset observations using novel mechanistic mathematical models.

Higher viral set points and $CD4^+CCR5^+$ T-cell depletion following transplantation and ATI are due to a reduction in SHIV-specific immunity. To understand why transplantation may have an effect on plasma viral load and $CD4^+CCR5^+$ T cell kinetics during ATI, we modified our mathematical model to include SHIV infection as described in **Fig. 1D** (**Methods**). Using model selection theory based on AIC, we found that the most parsimonious model to explain the data was the one without the dashed lines in **Fig. 1D** (**Table S2**). The best fit model simultaneously recapitulates plasma viral rebound and the kinetics of $CD4^+$ $CCR5^+$ and $CCR5^-$ T cells in each animal as shown in **Fig. 4E** and **Fig. S3** with corresponding estimated parameters in **Table 1** and **Table S5-S6**. In the best fit model, SHIV-specific $CD8^+$ effector cells reduce virus production in a non-cytolytic manner[58-60], possibly by secretion of HIV-antiviral factors[61-64]—not included in the model. Additionally, the model suggests that infection leads to enhanced activation of $CD4^+CCR5^-$ T cells leading to replenishment of $CD4^+CCR5^+$ T cells, explaining the concentration reduction of the $CD4^+CCR5^-$ compartment after ATI[65-68].

From the estimated parameters, only SHIV-based $CD8^+$ proliferation rate, ω_8, correlated positively with post-ATI $CD4^+CCR5^+$ T-cell nadir and negatively with viral load set point (**Fig. 5A-B**). We also found that the estimated SHIV-based $CD8^+$ proliferation rate was significantly lower in the transplant group, and the estimated time to viral rebound (Δ_t) was significantly higher in the transplant group (**Fig. 5C-D**). The projected fraction of SHIV-specific $CD8^+$ T cells in the transplant group approached zero (**Fig. S5**). Overall, these results suggest that a lower nadir of $CD4^+CCR5^+$ T cells and a higher viral load after ATI in transplanted animals is due to a loss of the immune response to SHIV-infected cells.

Greater loss of immunologic control during TBI/transplant requires higher numbers of CCR5-edited HSPCs to control viral rebound after ATI. To calculate the minimum threshold of CCR5-edited cells necessary to induce cART-independent virus suppression, we added a population of transplanted, gene-edited CCR5 HSPCs to our complete, fitted model of T cell subset and viral dynamics. We assumed that in the infused product there is a fraction f_p of HSPCs that have a biallelically-modified CCR5 gene and do not express CCR5. In the model we added state variables for protected progenitors and $CD4^+CCR5^-$ T cells that cannot become $CD4^+CCR5^+$ T cells (**Fig. 1E**, full model in **Supp. Materials**).

We simulated the model using parameter values obtained from the best fit in the previous section for each animal in the transplant group using 100 values of f_p from zero to one (0-100% CCR5-edited HSPCs). The minimal initial fraction to achieve post-rebound viral control was dependent on the underlying viral and immune dynamics of the given animal. For example, **Fig. 6A** depicts projections of the model using the best estimates from the fits of the model to transplanted animal Z09144 using six values of f_p: an initial fraction of protected cells smaller

than or equal to 40% will not lead to post-rebound viral control after ATI, even after a year. However, when f_p is 60% or greater than 80% it is possible to have a spontaneous post-rebound viral control at ~40 weeks and 10 weeks after ATI respectively. In both cases, a period of high-level viremia occurs prior to control.

The heatmaps in **Fig. 6B-E** show plasma viral load projections over 2 years after the start of ATI for different values of f_p. The model predicts that the minimum f_p to maintain post-rebound control for 2 years after ATI is higher for animals with lower estimated SHIV-specific immune response rates. For the two animals in the transplant group with lower viral setpoints, the minimum f_p for viral control was 35% and 19% (**Fig. 6D-E**). In contrast, for the other two animals, the minimum f_p for viral control was 56% and 97% (**Fig. 6B-C**). These model projections suggest that a larger loss of immunologic control during TBI/HSPC transplant results in a higher fraction of CCR5 gene-edited cells required for control of viral rebound after ATI.

The model also predicts that for some values of f_p it is possible to have two viral load stages after ATI: a temporary high viral set point in the first weeks after ATI may be followed by a delayed ART-free viral remission stage (e.g. when f_p is between 60% and 70% in **Fig. 6B** or between 5% and 20% in **Fig. 6E**). Therefore, in some cases the viral load set point determined during the initial weeks after ATI might not be a sufficient surrogate to predict viral control further in the future. On the other hand, when we project the $CD4^+CCR5^+$ T cell count for the same example in **Fig. 6A** we find that this cell subset does not undergo a significant change between weeks 2 and 10 after ATI for different scenarios of f_p (**Fig. 7A**). Moreover, the maximum decrease of $CD4^+CCR5^+$ T cells observed during the first 10 weeks after ATI is predicted to have a linear relationship with the minimum initial fraction of protected cells required to obtain post-rebound control after 2 years **(Fig. 7B)**. Therefore, the maximum initial

299 change in $CD4^+CCR5^+$ T cells 10 weeks after ATI, as well as the observed experimental value
300 for $f_{p,}$ might predict late viral control.

301 ## Discussion

302 Here we introduce a data-validated mathematical model that to our knowledge is the first
303 to simultaneously recapitulate SHIV viral loads, and $CD4^+$ and $CD8^+$ T cell subset counts during
304 HIV or SHIV infection. We systematically selected from a series of models to arrive at a set of
305 equations that most parsimoniously explains the available data. We recapitulated (1) peripheral
306 $CD4^+$ and $CD8^+$ T-cell subset reconstitution dynamics following transplant, and (2) T-cell
307 dynamics and SHIV viral rebound following ATI. Before ATI, all animals suppressed plasma
308 viral load below the limit of detection, allowing analysis of T cell reconstitution dynamics
309 independent of virus-mediated pressure. At each step, we applied model selection theory to
310 select the simplest set of mechanisms capable of explaining the observed data[57].

311 The model predicts that post-rebound viral control might be possible during autologous
312 gene-edited HSPC transplantation if therapy achieves (1) a sufficient fraction of gene-protected,
313 autologous HSPCs, and (2) maintenance or enhancement of SHIV-specific immune responses
314 following transplantation. Specifically, the model predicts that increasing amounts of
315 conditioning regimen-dependent depletion of the SHIV-specific immune response leads to a
316 higher threshold of CCR5-gene-edited cells in the transplanted HSPC product that is required to
317 obtain stable, ART-free viral control. These results are consistent with the cure achieved by the
318 Berlin patient who received transplant with 100% HIV-resistant cells after intense
319 conditioning[4,5]. In the autologous setting where 100% CCR5 editing may not be feasible,
320 adjunctive measures that augment virus-specific immunity, such as therapeutic vaccination,

infusion of HIV-specific CAR T cells or use of neutralizing antibodies, may synergize with HSPC transplantation to achieve post-treatment control[11,69].

The best model predicts that the lack of complete elimination of lymphocytes by TBI prevents $CD4^+CCR5^-$ cells from predominating post-transplant: the rapid expansion of $CD4^+CCR5^+$ and $CD8^+$ T cells during the first few weeks after HSPC transplantation is most likely due to lymphopenia-induced proliferation of remaining cells after TBI via a thymus-independent pathway; the slower expansion of $CD4^+CCR5^-$ T cells is due to thymic export of both transplanted and remaining cells. An important future research question will be to identify anatomic sites and mechanisms that allow activated $CD4^+CCR5^+$ to survive conditioning.

A challenge is that more intense conditioning may decrease remaining $CD4^+CCR5^+$ cells but will also lower SHIV specific immunity. We previously demonstrated the link between disruption of the immune response during transplant and increased magnitude of viral rebound during treatment interruption[14,51]. Here we predict that the magnitude of the SHIV-specific immune response is correlated not only with viral load set point, but also with the reduction of $CD4^+CCR5^+$ T cells after ATI. $CD4^+CCR5^+$ T cell depletion might also be predictive of the loss of depletion of virus-specific immunity following conditioning.

A final important observation from the model is that viral control may be delayed beyond the first ten weeks after ATI, and instead occur many months after ATI. Thus, viral load levels during the initial weeks after ATI may not completely define success (stable ART-free remission), whereas $CD4^+CCR5^+$ T-cell nadir should more strongly correlate with the degree of depletion of virus-specific immunity. In this sense, minimal $CD4^+CCR5^+$ T-cell nadir may predict post-rebound viral control, if the starting fraction of protected cells is known.

Our results are limited by a small sample size of eight animals. For that reason, several model parameters were assumed to be the same among the population (i.e., without random effects). However, the number of observations for each animal was large enough to discriminate among different plausible model candidates. Therefore, we performed projections using only the individual estimated parameters. Reassuringly, our results align with prior mechanistic studies of cellular reconstitution after stem cell transplantation[18,26,38,70,71]. Our analysis also suggests that the majority of reconstituting $CD4^+CCR5^-$ T cells do not proliferate and have a slow expansion that concurs with estimates of thymic export from previous studies[26,70,71].

The interplay between reconstituting HIV susceptible $CD4^+$ T cells, HIV-resistant $CD4^+$ T cells, infected cells, virus-specific immune cells, and replicating virus following autologous, CCR5-edited HPSC transplantation is extremely complex. Our results illustrate the capabilities of mathematical models to glean insight from this system and highlight that modeling will be required to optimize strategies for HIV cure studies, both in the macaque model, as well as in HIV^+ individuals.

Acknowledgements

This study was supported by grants from the National Institutes of Health, National Institute of Allergy and Infectious Diseases (UM1 AI126623). ERD is supported by the National Center for Advancing Translational Sciences of the National Institutes of Health under Award Number KL2 TR002317. DBR is supported by a Washington Research Foundation postdoctoral fellowship, and a CFAR NIA P30 AI027757. The funders had no role in study design, data collection and analysis, decision to publish, or preparation of the manuscript. The content is solely the responsibility of the authors and does not necessarily represent the official views of the National Institutes of Health or the Washington Research Foundation.

Authorship Contributions

E.F.C. and J.T.S. conceived the study. C.W.P. and H.P.K. contributed ideas and data sources for the project. E.R.D. and D.B.R. contributed ideas for the development of mechanistic mathematical models. B.T.M. contributed ideas and support for statistical models and analyzes. E.F.C. assembled data, wrote all code, performed all calculations and derivations, ran the models, and analyzed output data. J.T.S. and E.F.C. wrote the manuscript with contributions from all other authors.

Disclosure of Conflicts of Interest

The authors declare no competing financial interests.

Animal Welfare.

The data used in this work were collected in strict accordance with the recommendations in the *Guide for the Care and Use of Laboratory Animals* of the National Institutes of Health. The study protocol was approved by the Institutional Animal Care and Use Committees (3235-03) of the Fred Hutchinson Cancer Research Center and the University of Washington.

Tables

Table 1. Parameters of the model. Values are from steady state equations, using population estimates from best model fits or assumed from the references as described. When assumed from steady state equations, population estimates were used. See **Supp. Materials** for more details.

Parameter	Units	Description	Value		Source
			Control	Transplant	
$T(t_0)$	cells	Number of cells in the transplant product.	0	$4*10^7$	Fixed, assumed from reference [14].
$P(t_0)$	cells	Number of cells in the BM/Thymus at the moment of transplant.	$4*10^8$	0	Control: Computed from the median of steady state equations. Transplant: Fixed, assumed.
$N(t_0)$	cells/μL	Blood $CD4^+CCR5^-$ T cell concentration at the moment of transplant.	1249	47	Control: Computed from the median of steady state equations. Transplant: Fitted.
$S(t_0)$	cells/μL	Blood $CD4^+CCR5^+$ T cell concentration at the moment of transplant.	115	2	Control: Computed from the median of steady state equations. Transplant: Fitted.
$M(t_0)$	cells/μL	Blood $CD8^+$ T_N + T_{CM} cell concentration at the moment of transplant.	305	8	Control: Computed from the median of steady state equations. Transplant: Fitted.
$E(t_0)$	cells/μL	Blood $CD8^+$ T_{EM} cell concentration at the moment of transplant.	935	17	Control: Computed from the median of steady state equations. Transplant: Fitted.
$E_h(t_0)$	cells/μL	Blood SHIV-specific $CD8^+$ T effector cell concentration at the moment of transplant.	0	0	Control: Computed from steady state equations. Transplant: Assumed.
$I_p(t_0)$	cells/μL	Productively infected blood $CD4^+CCR5^+$ T cell	$2*10^{-6}$	$2*10^{-6}$	Computed from steady state equations.

		concentration at the moment of transplant.			
$I_u(t_0)$	cells/μL	Unproductively infected blood $CD4^+CCR5^+$ T cell concentration at the moment of transplant.	0	0	Computed from steady state equations.
$V(t_0)$	RNA copies/mL	Plasma viral load at the moment of transplant.	0.5	0.5	Computed from steady state equations.
k_e	1/day	Homing rate of transplanted cells into the bone marrow.	1		Fixed, assumed from references [72,73].
$\hat{r}_p = r_p - \lambda_p - d_p$	1/day	Renewal rate of stem and progenitor cells in the bone marrow/thymus.	0.04		Fitted.
$\hat{r}_s = r_s - d_s$	1/day	Proliferation rate of blood $CD4^+CCR5^+$ T cells.	0.14		Fitted.
$\hat{r}_m = r_m - \lambda_m - d_m$	1/day	Proliferation rate of blood $CD8^+$ T_N + T_{CM} cells.	0.003		Fitted.
$\hat{r}_e = r_e - d_e$	1/day	Proliferation rate of $CD8^+$ T_{EM} cells.	0.09		Fitted.
$\hat{d}_n = \lambda_n + d_n$	1/day	Removal rate of blood $CD4^+CCR5^-$ T cells.	0.01		Fitted.
$\lambda_p = \lambda_e = \lambda_f$	1/day	Thymic output rate of T cells.	0.01		Fitted.
λ_n	1/day	CCR5 upregulation rate in $CD4^+$ T cells.	0.004		Fitted.
λ_m	1/day	Differentiation rate of $CD8^+$ T_N + T_{CM} cells to $CD8^+$ T_{EM} cells.	0.09		Fitted.
$K_p = K\frac{\bar{r}_p}{r_p}$	cells/μL	Effective carrying capacity of progenitor cells.	1664		Fitted.
$K_s = K\frac{\bar{r}_s}{r_s}$	cells/μL	Effective carrying capacity of $CD4^+CCR5^+$ T cells.	1328		Fitted.
$K_m = K\frac{\bar{r}_m}{r_m}$	cells/μL	Effective carrying capacity of $CD8^+$ T_N + T_{CM} cells.	49		Fitted.

$K_e = K\frac{\bar{r}_e}{r_e}$	cells/μL	Effective carrying capacity of $CD8^+$ T_{EM} cells.	1257	Fitted.
β	μL/ copies/day	Infectivity rate.	0.0003	Fitted.
Δ_t	days	Time to rebound after ATI.	7.5	Fitted.
δ_I	1/day	Death rate of infected $CD4^+CCR5^+$ T cells.	1	Fixed, assumed using estimates from references [74,75].
τ	-	Fraction of infected cell that produce infectious virus.	0.05	Fixed, assumed from reference [54].
$\xi\bar{L}$	cells/μL/day	Number of latent cells that activate per day.	$2*10^{-7}$	Fixed, assumed to have a viral load of ~0.5 copies/mL during cART.
π	1/day	Viral production rate.	$5*10^4$	Fixed, assumed using estimates from reference [76].
γ	1/day	Virus clearance rate.	23	Fixed, assumed using estimates from reference [77].
ω_4	μL/cells/day	SHIV-dependent replenishment of $CD4^+CCR5^+$ T cells.	0.19	Fitted.
ω_8	μL/cells/day	SHIV-dependent proliferation rate of $CD8^+$ T cells.	0.002	Fitted.
I_{50}	cells/μL	50% maximum value of adaptive infected cells, allows bounded growth.	0.20	Fitted.
f	-	Fraction of SHIV-$CD8^+$-responding cells that become SHIV-specific effectors.	0.9	Fixed, assumed from reference [46].
d_h	1/day	Death rate of SHIV-specific effector $CD8^+$ T cells.	0.05	Fitted.
$\frac{1}{\theta}$	μL/cells	50% maximum value of SHIV-specific immune cells to block virus production.	1	Fixed.

385

References

1. Chun T-W, Carruth L, Finzi D, et al. Quantification of latent tissue reservoirs and total body viral load in HIV-1 infection. *Nature*. 1997;387(6629):183.
2. Chun T-W, Finzi D, Margolick J, Chadwick K, Schwartz D, Siliciano RF. In vivo fate of HIV-1-infected T cells: Quantitative analysis of the transition to stable latency. *Nature Medicine*. 1995;1(12):1284-1290.
3. Finzi D, Hermankova M, Pierson T, et al. Identification of a Reservoir for HIV-1 in Patients on Highly Active Antiretroviral Therapy. *Science*. 1997;278(5341):1295-1300.
4. Allers K, Hütter G, Hofmann J, et al. Evidence for the cure of HIV infection by CCR5Δ32/Δ32 stem cell transplantation. *Blood*. 2011;117(10):2791-2799.
5. Hütter G, Nowak D, Mossner M, et al. Long-Term Control of HIV by CCR5 Delta32/Delta32 Stem-Cell Transplantation. *New England Journal of Medicine*. 2009;360(7):692-698.
6. Gupta RK, Abdul-jawad S, McCoy LE, et al. HIV-1 remission following CCR5Δ32/Δ32 haematopoietic stem-cell transplantation. *Nature*. 2019:1.
7. Henrich TJ, Hanhauser E, Harrison LJ, et al. CCR5-Δ32 Heterozygosity, HIV-1 Reservoir Size, and Lymphocyte Activation in Individuals Receiving Long-term Suppressive Antiretroviral Therapy. *The Journal of Infectious Diseases*. 2016;213(5):766-770.
8. Henrich TJ, Hanhauser E, Marty FM, et al. Antiretroviral-Free HIV-1 Remission and Viral Rebound After Allogeneic Stem Cell Transplantation: Report of 2 Cases. *Annals of Internal Medicine*. 2014;161(5):319.
9. Henrich TJ, Hu Z, Li JZ, et al. Long-Term Reduction in Peripheral Blood HIV Type 1 Reservoirs Following Reduced-Intensity Conditioning Allogeneic Stem Cell Transplantation. *The Journal of Infectious Diseases*. 2013;207(11):1694-1702.
10. Salgado M, Kwon M, Gálvez C, et al. Mechanisms That Contribute to a Profound Reduction of the HIV-1 Reservoir After Allogeneic Stem Cell Transplant. *Annals of Internal Medicine*. 2018.
11. Haworth KG, Peterson CW, Kiem H-P. CCR5-edited gene therapies for HIV cure: Closing the door to viral entry. *Cytotherapy*. 2017;19(11):1325-1338.
12. Tebas P, Stein D, Tang WW, et al. Gene Editing of CCR5 in Autologous CD4 T Cells of Persons Infected with HIV. *New England Journal of Medicine*. 2014;370(10):901-910.
13. Peterson CW, Wang J, Norman KK, et al. Long-term multilineage engraftment of autologous genome-edited hematopoietic stem cells in nonhuman primates. *Blood*. 2016;127(20):2416-2426.
14. Peterson CW, Benne C, Polacino P, et al. Loss of immune homeostasis dictates SHIV rebound after stem-cell transplantation. *JCI Insight*. 2017;2(4).
15. Peterson CW, Haworth KG, Polacino P, et al. Lack of viral control and development of combination antiretroviral therapy escape mutations in macaques after bone marrow transplantation. *Aids*. 2015;29(13):1597-1606.
16. Peterson CW, Wang J, Deleage C, et al. Differential impact of transplantation on peripheral and tissue-associated viral reservoirs: Implications for HIV gene therapy. *PLOS Pathogens*. 2018;14(4):e1006956.
17. Ho O, Larsen K, Polacino P, et al. Pathogenic infection of Macaca nemestrinawith a CCR5-tropic subtype-C simian-human immunodeficiency virus. *Retrovirology*. 2009;6(1):65.

18. Jameson SC. Maintaining the norm: T-cell homeostasis. *Nature Reviews Immunology*. 2002;2(8):547-556.
19. Mehr R, Perelson AS. Blind T-cell homeostasis and the CD4/CD8 ratio in the thymus and peripheral blood. *Journal of Acquired Immune Deficiency Syndromes and Human Retrovirology: Official Publication of the International Retrovirology Association*. 1997;14(5):387-398.
20. Margolick JB, Donnenberg AD. T-cell homeostasis in HIV-1 infection. *Seminars in Immunology*. 1997;9(6):381-388.
21. Schluns KS, Williams K, Ma A, Zheng XX, Lefrançois L. Cutting Edge: Requirement for IL-15 in the Generation of Primary and Memory Antigen-Specific CD8 T Cells. *The Journal of Immunology*. 2002;168(10):4827-4831.
22. Schluns KS, Kieper WC, Jameson SC, Lefrançois L. Interleukin-7 mediates the homeostasis of naïve and memory CD8 T cells *in vivo*. *Nature Immunology*. 2000;1(5):426-432.
23. Goldrath AW, Luckey CJ, Park R, Benoist C, Mathis D. The molecular program induced in T cells undergoing homeostatic proliferation. *Proceedings of the National Academy of Sciences*. 2004;101(48):16885-16890.
24. Voehringer D, Liang H-E, Locksley RM. Homeostasis and Effector Function of Lymphopenia-Induced "Memory-Like" T Cells in Constitutively T Cell-Depleted Mice. *The Journal of Immunology*. 2008;180(7):4742-4753.
25. Boyman O, Létourneau S, Krieg C, Sprent J. Homeostatic proliferation and survival of naïve and memory T cells. *European Journal of Immunology*. 2009;39(8):2088-2094.
26. Douek DC, Vescio RA, Betts MR, et al. Assessment of thymic output in adults after haematopoietic stemcell transplantation and prediction of T-cell reconstitution. *The Lancet*. 2000;355(9218):1875-1881.
27. Douek DC, McFarland RD, Keiser PH, et al. Changes in thymic function with age and during the treatment of HIV infection. *Nature*. 1998;396(6712):690-695.
28. Bender J, Mitchell T, Kappler J, Marrack P. Cd4+ T Cell Division in Irradiated Mice Requires Peptides Distinct from Those Responsible for Thymic Selection. *Journal of Experimental Medicine*. 1999;190(3):367-374.
29. Kieper WC, Jameson SC. Homeostatic expansion and phenotypic conversion of naïve T cells in response to self peptide/MHC ligands. *Proceedings of the National Academy of Sciences*. 1999;96(23):13306-13311.
30. Sallusto F, Geginat J, Lanzavecchia A. Central Memory and Effector Memory T Cell Subsets: Function, Generation, and Maintenance. *Annual Review of Immunology*. 2004;22(1):745-763.
31. Saout CL, Mennechet S, Taylor N, Hernandez J. Memory-like CD8+ and CD4+ T cells cooperate to break peripheral tolerance under lymphopenic conditions. *Proceedings of the National Academy of Sciences*. 2008;105(49):19414-19419.
32. Sprent J, Surh CD. Normal T cell homeostasis: the conversion of naive cells into memory-phenotype cells. *Nature Immunology*. 2011;12(6):478-484.
33. Takeda S, Rodewald H-R, Arakawa H, Bluethmann H, Shimizu T. MHC Class II Molecules Are Not Required for Survival of Newly Generated CD4+ T Cells, but Affect Their Long-Term Life Span. *Immunity*. 1996;5(3):217-228.
34. Tanchot C, Lemonnier FA, Pérarnau B, Freitas AA, Rocha B. Differential Requirements for Survival and Proliferation of CD8 Naïve or Memory T Cells. *Science*. 1997;276(5321):2057-2062.

35. Fry TJ, Mackall CL. Interleukin-7: master regulator of peripheral T-cell homeostasis? *Trends in Immunology*. 2001;22(10):564-571.
36. Tan JT, Dudl E, LeRoy E, et al. IL-7 is critical for homeostatic proliferation and survival of naïve T cells. *Proceedings of the National Academy of Sciences*. 2001;98(15):8732-8737.
37. Yamaki S, Ine S, Kawabe T, et al. OX40 and IL-7 play synergistic roles in the homeostatic proliferation of effector memory CD4+ T cells. *European Journal of Immunology*. 2014;44(10):3015-3025.
38. Guillaume T, Rubinstein DB, Symann M. Immune Reconstitution and Immunotherapy After Autologous Hematopoietic Stem Cell Transplantation. *Blood*. 1998;92(5):1471-1490.
39. Spits H. Development of αβ T cells in the human thymus. *Nature Reviews Immunology*. 2002;2(10):760.
40. Berkowitz RD, Beckerman KP, Schall TJ, McCune JM. CXCR4 and CCR5 Expression Delineates Targets for HIV-1 Disruption of T Cell Differentiation. *The Journal of Immunology*. 1998;161(7):3702-3710.
41. Bleul CC, Wu L, Hoxie JA, Springer TA, Mackay CR. The HIV coreceptors CXCR4 and CCR5 are differentially expressed and regulated on human T lymphocytes. *Proceedings of the National Academy of Sciences*. 1997;94(5):1925-1930.
42. Zaitseva MB, Lee S, Rabin RL, et al. CXCR4 and CCR5 on Human Thymocytes: Biological Function and Role in HIV-1 Infection. *The Journal of Immunology*. 1998;161(6):3103-3113.
43. Buchholz VR, Flossdorf M, Hensel I, et al. Disparate Individual Fates Compose Robust CD8+ T Cell Immunity. *Science*. 2013;340(6132):630-635.
44. Farber DL, Yudanin NA, Restifo NP. Human memory T cells: generation, compartmentalization and homeostasis. *Nature Reviews Immunology*. 2014;14(1):24-35.
45. Kaech SM, Wherry EJ, Ahmed R. Effector and memory T-cell differentiation: implications for vaccine development. *Nature Reviews Immunology*. 2002;2(4):251-262.
46. Borducchi EN, Cabral C, Stephenson KE, et al. Ad26/MVA therapeutic vaccination with TLR7 stimulation in SIV-infected rhesus monkeys. *Nature*. 2016;540(7632):284.
47. De Boer RJ. Understanding the Failure of CD8+ T-Cell Vaccination against Simian/Human Immunodeficiency Virus. *Journal of Virology*. 2007;81(6):2838-2848.
48. Hill AL, Rosenbloom DIS, Nowak MA, Siliciano RF. Insight into treatment of HIV infection from viral dynamics models. *Immunological Reviews*. 2018;285(1):9-25.
49. Perelson AS. Modelling viral and immune system dynamics. *Nature Reviews Immunology*. 2002;2(1):28-36.
50. Perelson AS, Essunger P, Cao Y, et al. Decay characteristics of HIV-1-infected compartments during combination therapy. *Nature*. 1997;387(6629):188.
51. Reeves DB, Peterson CW, Kiem H-P, Schiffer JT. Autologous Stem Cell Transplantation Disrupts Adaptive Immune Responses during Rebound Simian/Human Immunodeficiency Virus Viremia. *Journal of Virology*. 2017;91(13):e00095-00017.
52. Wodarz D, Garg N, Komarova NL, et al. Kinetics of CLL cells in tissues and blood during therapy with the BTK inhibitor ibrutinib. *Blood*. 2014;123(26):4132-4135.
53. Wodarz D, Nowak MA. Specific therapy regimes could lead to long-term immunological control of HIV. *Proceedings of the National Academy of Sciences*. 1999;96(25):14464-14469.
54. Doitsh G, Cavrois M, Lassen KG, et al. Abortive HIV Infection Mediates CD4 T Cell Depletion and Inflammation in Human Lymphoid Tissue. *Cell*. 2010;143(5):789-801.

55. Matrajt L, Younan PM, Kiem H-P, Schiffer JT. The Majority of CD4+ T-Cell Depletion during Acute Simian-Human Immunodeficiency Virus SHIV89.6P Infection Occurs in Uninfected Cells. *Journal of Virology*. 2014;88(6):3202-3212.
56. Lavielle M. Mixed Effects Models for the Population Approach: Models, Tasks, Methods and Tools (ed 1 edition). Boca Raton: Chapman and Hall/CRC; 2014.
57. Burnham KP, Anderson DR. Model Selection and Multimodel Inference: A Practical Information-Theoretic Approach (ed 2). New York: Springer-Verlag; 2002.
58. Elemans M, Basatena N-KSa, Klatt NR, Gkekas C, Silvestri G, Asquith B. Why Don't CD8+ T Cells Reduce the Lifespan of SIV-Infected Cells In Vivo? *PLOS Computational Biology*. 2011;7(9):e1002200.
59. Klatt NR, Shudo E, Ortiz AM, et al. CD8+ Lymphocytes Control Viral Replication in SIVmac239-Infected Rhesus Macaques without Decreasing the Lifespan of Productively Infected Cells. *PLOS Pathogens*. 2010;6(1):e1000747.
60. Wong JK, Strain MC, Porrata R, et al. In Vivo CD8+ T-Cell Suppression of SIV Viremia Is Not Mediated by CTL Clearance of Productively Infected Cells. *PLOS Pathogens*. 2010;6(1):e1000748.
61. Shridhar V, Chen Y, Gupta P. The CD8 Antiviral Factor (CAF) can suppress HIV-1 transcription from the Long Terminal Repeat (LTR) promoter in the absence of elements upstream of the CATATAA box. *Virology Journal*. 2014;11(1):130.
62. Blazek D, Teque F, Mackewicz C, Peterlin M, Levy JA. The CD8+ cell non-cytotoxic antiviral response affects RNA polymerase II-mediated human immunodeficiency virus transcription in infected CD4+ cells. *Journal of General Virology*. 2016;97(1):220-224.
63. Zhang L, Yu W, He T, et al. Contribution of Human α-Defensin 1, 2, and 3 to the Anti-HIV-1 Activity of CD8 Antiviral Factor. *Science*. 2002;298(5595):995-1000.
64. Levy JA, Mackewicz CE, Barker E. Controlling HIV pathogenesis: the role of the noncytotoxic anti-HIV response of CD8+ T cells. *Immunology Today*. 1996;17(5):217-224.
65. A. OA, J. PL. CD4+ T□cell depletion in HIV infection: mechanisms of immunological failure. *Immunological Reviews*. 2013;254(1):54-64.
66. Douek DC, Picker LJ, Koup RA. T Cell Dynamics in HIV-1 Infection. *Annual Review of Immunology*. 2003;21(1):265-304.
67. Okoye A, Meier-Schellersheim M, Brenchley JM, et al. Progressive CD4+ central–memory T cell decline results in CD4+ effector–memory insufficiency and overt disease in chronic SIV infection. *Journal of Experimental Medicine*. 2007;204(9):2171-2185.
68. Okoye AA, Rohankhedkar M, Abana C, et al. Naive T cells are dispensable for memory CD4+ T cell homeostasis in progressive simian immunodeficiency virus infection. *Journal of Experimental Medicine*. 2012;209(4):641-651.
69. Zhen A, Peterson CW, Carrillo MA, et al. Long-term persistence and function of hematopoietic stem cell-derived chimeric antigen receptor T cells in a nonhuman primate model of HIV/AIDS. *PLOS Pathogens*. 2017;13(12):e1006753.
70. Krenger W, Blazar BR, Holländer GA. Thymic T-cell development in allogeneic stem cell transplantation. *Blood*. 2011;117(25):6768-6776.
71. Roux E, Dumont-Girard F, Starobinski M, et al. Recovery of immune reactivity after T-cell–depleted bone marrow transplantation depends on thymic activity. *Blood*. 2000;96(6):2299-2303.
72. Lapidot T, Dar A, Kollet O. How do stem cells find their way home? *Blood*. 2005;106(6):1901-1910.

73. Chute J. Stem cell homing. *Current Opinion in Hematology*. 2006;13(6):399-406.
74. Markowitz M, Louie M, Hurley A, et al. A Novel Antiviral Intervention Results in More Accurate Assessment of Human Immunodeficiency Virus Type 1 Replication Dynamics and T-Cell Decay In Vivo. *Journal of Virology*. 2003;77(8):5037-5038.
75. Cardozo EF, Andrade A, Mellors JW, Kuritzkes DR, Perelson AS, Ribeiro RM. Treatment with integrase inhibitor suggests a new interpretation of HIV RNA decay curves that reveals a subset of cells with slow integration. *PLOS Pathogens*. 2017;13(7):e1006478.
76. Chen HY, Mascio MD, Perelson AS, Ho DD, Zhang L. Determination of virus burst size in vivo using a single-cycle SIV in rhesus macaques. *Proceedings of the National Academy of Sciences*. 2007;104(48):19079-19084.
77. Ramratnam B, Bonhoeffer S, Binley J, et al. Rapid production and clearance of HIV-1 and hepatitis C virus assessed by large volume plasma apheresis. *The Lancet*. 1999;354(9192):1782-1785.

Figure Legends

Figure 1. Study design and mathematical modeling. A. Four animals were infected with SHIV, suppressed with cART and then underwent TBI/HSPC transplantation without editing of CCR5 (Transplant group). A control group of four animals did not receive TBI or HSPC transplantation. Both groups underwent ATI approximately one year after cART initiation. **B.** Mathematical modeling approach. **C.** Mathematical model for T cell reconstitution. Each circle represents a cell compartment: T represents the HSPCs from the transplant; P, the progenitor cells in bone marrow (BM) and Thymus; S and N, $CD4^+CCR5^+$ and $CD4^+CCR5^-$ T cells, respectively; M and E, the $CD8^+$ T cells with naïve and central memory phenotypes, and effector memory phenotypes, respectively. **D.** Mathematical model for virus dynamics. We adapted the previous model by including the following assumptions. Susceptible cells, S, are infected by the virus, V. I_p and I_u represent a fraction τ of the infected cells produce virus, I_p, and the other fraction become unproductively infected, I_u. Total $CD4^+CCR5^+$ T cell count is given by the sum of S, I_p and I_u. All infected cells die at rate δ_I. I_P cells arise from activation of latently infected cells at rate $\xi\bar{L}$, and produce virus at a rate π, that is cleared at rate γ. $CD8^+$ M cells proliferate in the presence of infection with rate ω_8 from which a fraction f become SHIV-specific $CD8^+$ effector T cells, E_h, that are removed at a rate d_h. These effector cells reduce virus production or infectivity by $1/(1+\theta E_h)$, or $1/(1+\varphi E_h)$, respectively. Non-susceptible $CD4^+$ T cells upregulate CCR5 in the presence of infection and replenish the susceptible pool with rate ω_4. **E.** Schematic of the extended mathematical model that includes CCR5-edited, protected cells. Protected cells from transplant: T_p, protected progenitor cells in bone marrow/thymus: P_p, and protected $CD4^+CCR5^-$ T cells: N_p are included. The initial fraction of protected cells is represented by the parameter f_p.

Figure 2. $CD4^+$ and $CD8^+$ T cell dynamics post-transplantation, pre-ATI. Range of blood **A.** $CD4^+$ and **B.** $CD8^+$ T cell counts using all data points for the period before ATI in control animals (p-value calculated with a paired t-test for averaged measurements post-transplant). **C.** Distribution of the growth rate estimates of $CD4^+CCR5^+$, $CD4^+CCR5^-$, and $CD8^+$ T cells using all data points from time of transplant until their levels reached set point in transplanted animals (p-value calculated using a paired t-test). We assumed set point as the data point after which the sum of consecutive changes from the moment of transplant in T cell counts was smaller or equal to zero. **D.** Empirical data for peripheral subset counts (colored data points) and best fits of the model (solid lines) to all blood T cell subsets before ATI for all animals in the transplant group. Each row is one animal.

Figure 3. Model predictions of the $CD4^+CCR5^+$ T cell turnover. Model prediction of the total concentration of $CD4^+CCR5^+$ T new cells generated by proliferation (solid line) and the concentration generated by up-regulation of CCR5 (dashed line) over time using the best estimates for all 4 transplanted animals.

Figure 4. Plasma viral load and $CD4^+$ T cell kinetics after ATI. A-D: Distributions of **A.** peak viral load post-ATI, **B.** viral load at endpoint necropsy, **C.** $CD4^+CCR5^+$ T-cell normalized nadir post-ATI relative to the CCR5 concentration at ATI, **D.** $CD4^+CCR5^-$ T-cell nadir post-ATI. P-values were calculated using Mann-Whitney test. **E.** Best fits of the model (black lines) to SHIV RNA, and blood $CD4^+CCR5^+$ T, $CD4^+CCR5^-$ T, total $CD8^+$ T, $CD8^+$ T_{EM}, and $CD8^+$ T_n and T_{CM} cell counts (colored data points) for all 4 transplanted animals.

Figure 5. Loss of SHIV-specific CD8 response after transplantation. Scatterplots of the SHIV-dependent CD8 proliferation rate (ω_8) vs. **A.** $CD4^+CCR5^+$ normalized nadir post-ATI relative to the CCR5 concentration at ATI, and **B.** final observed viral load from all animals; (p-values calculated using Spearman's rank test). **C-D:** Individual parameter estimates of **C.** the SHIV-dependent CD8 proliferation rate (ω_8) and **D.** the time of rebound after ATI (see text). Blue: control, and red: transplant groups (p-values calculated by Mann-Whitney test).

Figure 6. Model predictions for post-rebound viral control after CCR5 gene-edited HSPC transplant. A. Predictions for plasma viral load post-ATI using the adapted model for varying values of f_p (using parameter estimates from animal Z09144). **B-E.** Predictions for plasma viral load (heat-map color) for each animal at a given time post-ATI (x-axis) and a given f_p (y-axis).

Figure 7. $CD4^+CCR5^+$ T cell nadir as a predictor for necessary minimum initial fraction of protected cells to achieve post ATI control. A. Predictions for the normalized $CD4^+CCR5^+$ T cell counts relative to their concentration at ATI using the adapted model for varying values of f_p (using parameter estimates from animal Z09144). **B.** Predicted $CD4^+CCR5^+$ T cell normalized nadir during the first 10 weeks after ATI for the minimum fraction of protected cells required to obtain post-rebound control after 2 years using parameter estimates for each animal. Dashed line describes a linear regression of the computed minimum fraction of protected cells (f_p) and the CCR5 normalized nadir.

Predicted maximum decrease of $CD4^+CCR5^+$ T cells during the first 10 weeks after ATI for the minimum fraction of protected cells required to obtain post-rebound control after 2 years using parameter estimates for each animal

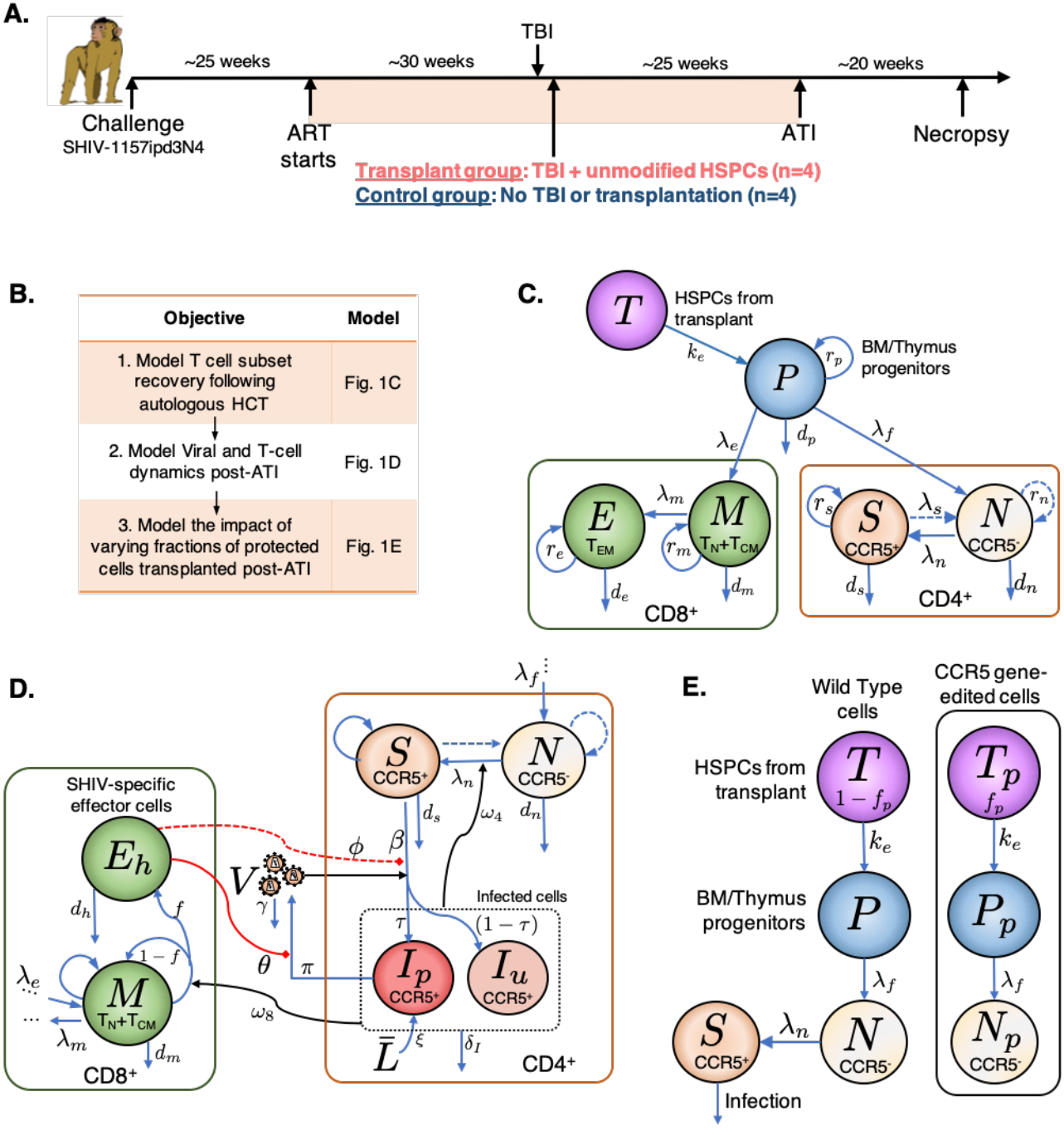
A.
TBI
~25 weeks
~30 weeks
~25 weeks
~20 weeks
Challenge
SHIV-1157ipd3N4
ART starts
ATI
Necropsy
Transplant group: TBI + unmodified HSPCs (n=4)
Control group: No TBI or transplantation (n=4)
B.
Objective
Model
1. Model T cell subset recovery following autologous HCT
Fig. 1C
2. Model Viral and T-cell dynamics post-ATI
Fig. 1D
3. Model the impact of varying fractions of protected cells transplanted post-ATI
Fig. 1E
C.
HSPCs from transplant
BM/Thymus progenitors
CD8+
CD4+
D.
SHIV-specific effector cells
Infected cells
CD8+
CD4+
E.
Wild Type cells
CCR5 gene-edited cells
HSPCs from transplant
BM/Thymus progenitors
Infection

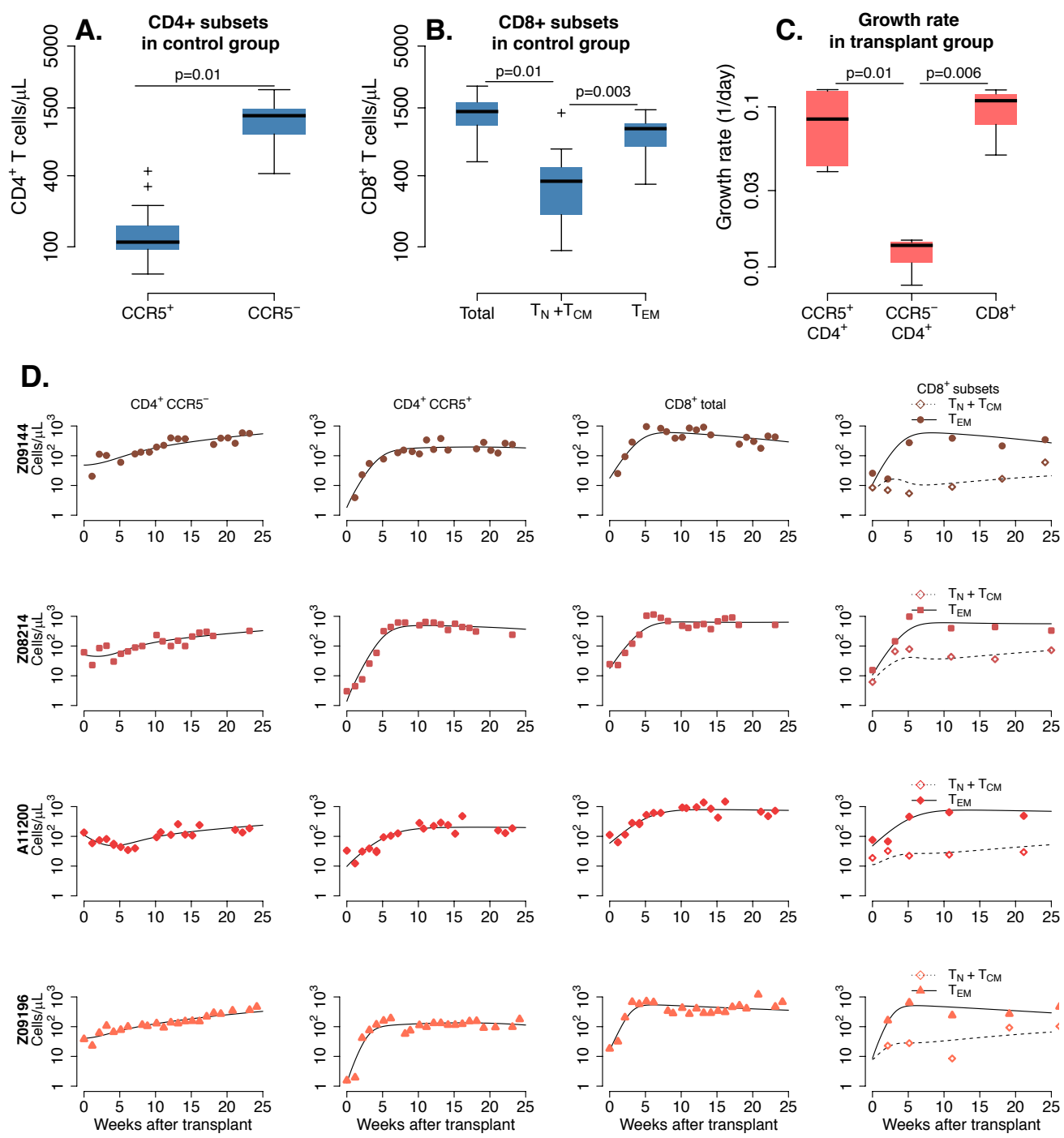
A.
CD4+ subsets in control group
p=0.01
CD4+ T cells/µL
100
400
1500
5000
CCR5+
CCR5−
B.
CD8+ subsets in control group
p=0.01
p=0.003
CD8+ T cells/µL
Total
TN +TCM
TEM
C.
Growth rate in transplant group
p=0.01
p=0.006
Growth rate (1/day)
0.01
0.03
0.1
CCR5+ CD4+
CCR5− CD4+
CD8+
D.
CD4+ CCR5−
CD4+ CCR5+
CD8+ total
CD8+ subsets
TN + TCM
TEM
Z09144
Z08214
A11200
Z09196
Cells/µL
1
10
10^2
10^3
0
5
10
15
20
25
Weeks after transplant

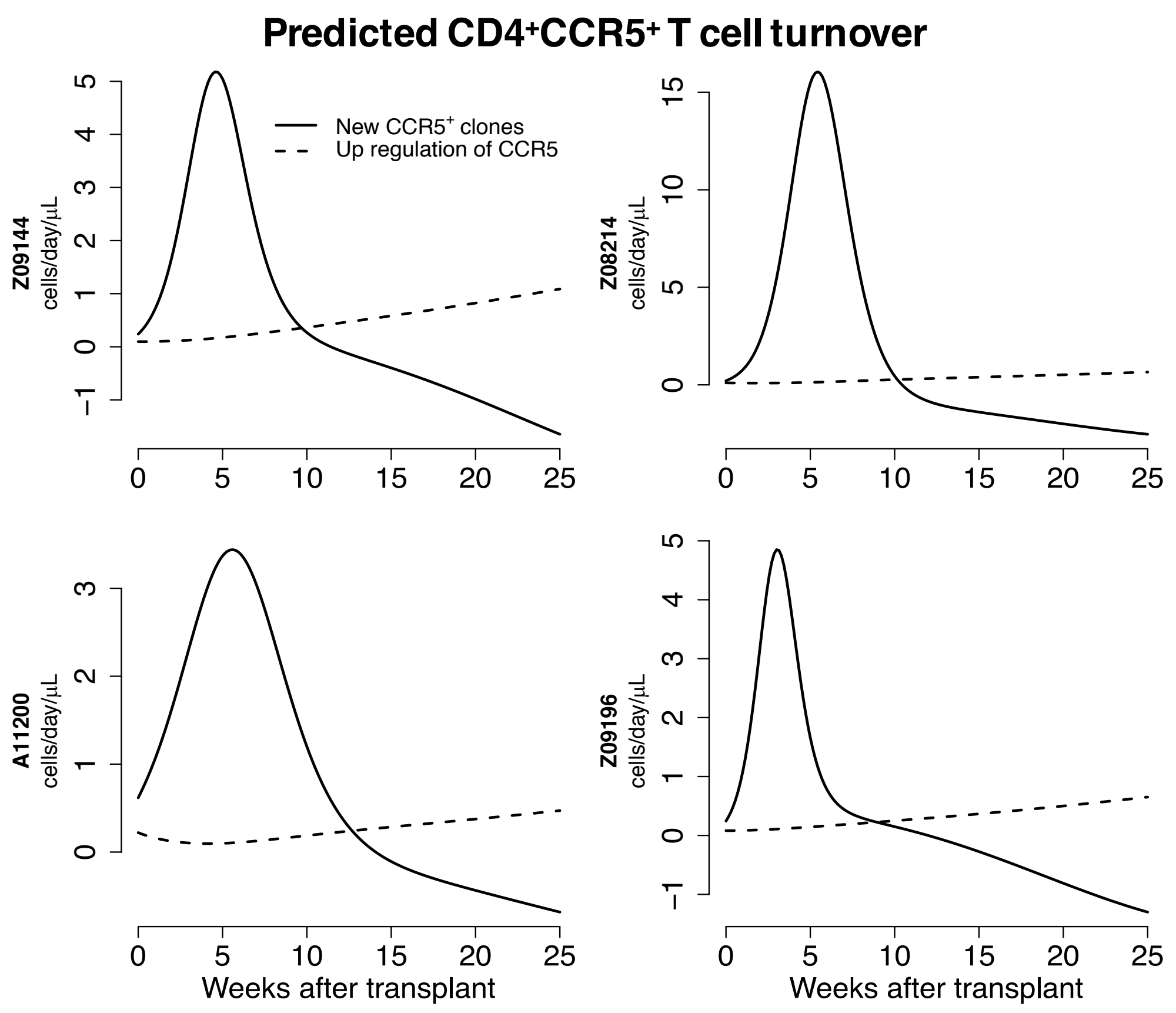
Predicted CD4+CCR5+ T cell turnover
New CCR5+ clones
Up regulation of CCR5
Z09144
cells/day/µL
Z08214
cells/day/µL
A11200
cells/day/µL
Z09196
cells/day/µL
Weeks after transplant
Weeks after transplant

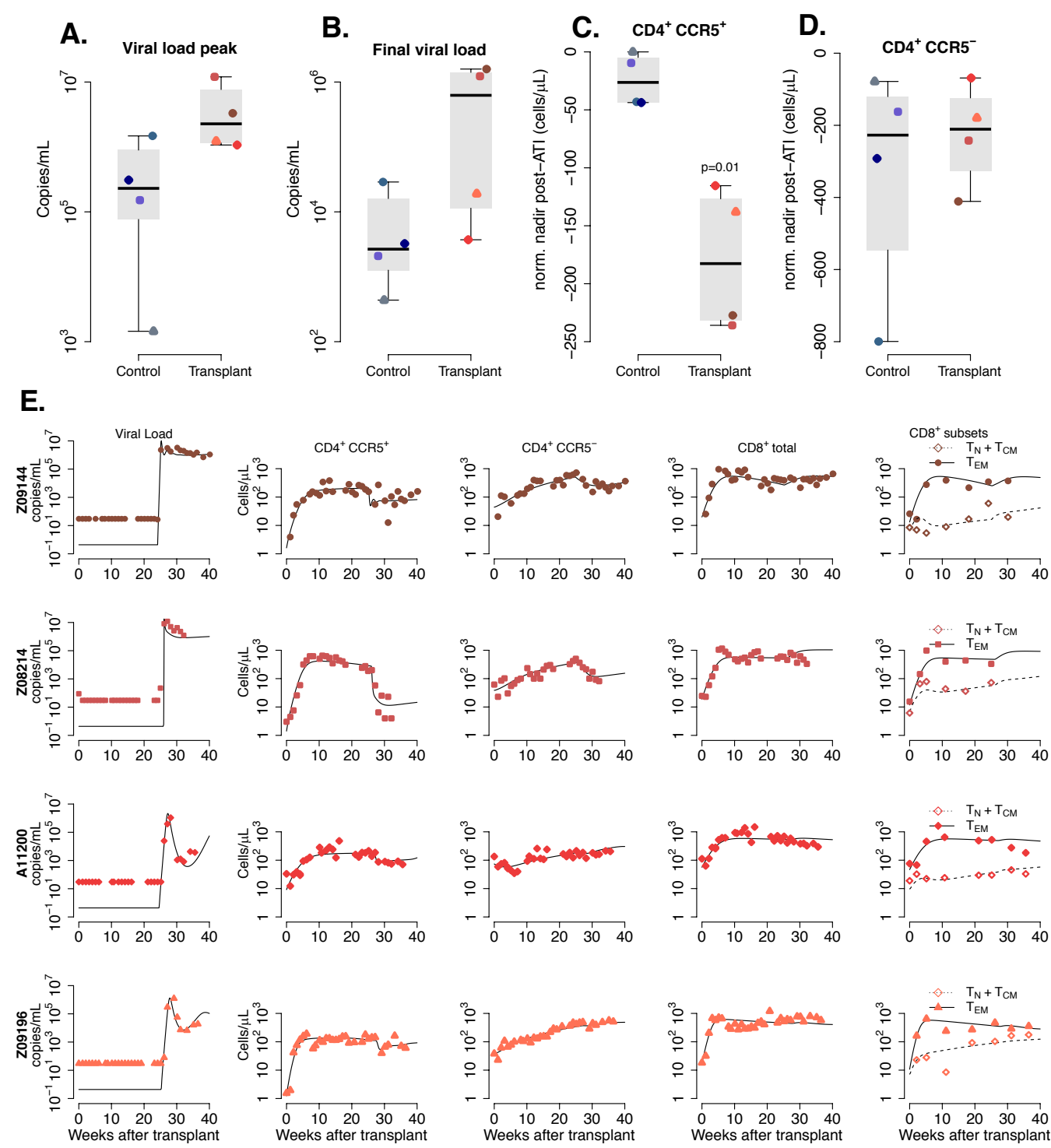
A.
Viral load peak
Copies/mL
Control
Transplant
B.
Final viral load
Copies/mL
Control
Transplant
C.
CD4+ CCR5+
norm. nadir post–ATI (cells/μL)
p=0.01
Control
Transplant
D.
CD4+ CCR5−
norm. nadir post–ATI (cells/μL)
Control
Transplant
E.
Viral Load
CD4+ CCR5+
CD4+ CCR5−
CD8+ total
CD8+ subsets
TN + TCM
TEM
Z09144
Z08214
A11200
Z09196
copies/mL
Cells/μL
Weeks after transplant

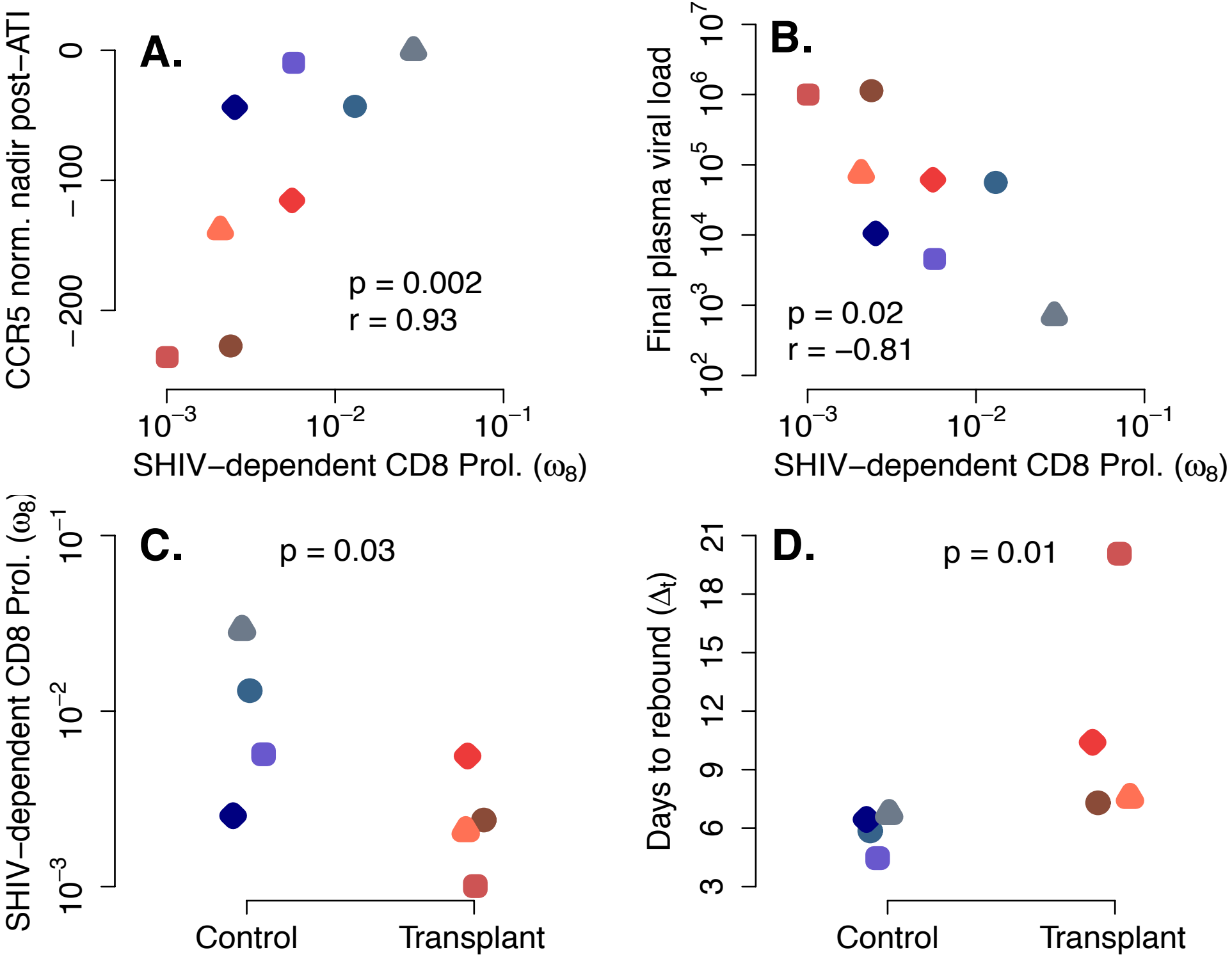
A.
CCR5 norm. nadir post–ATI
0
−100
−200
p = 0.002
r = 0.93
10^{-3}
10^{-2}
10^{-1}
SHIV–dependent CD8 Prol. (ω_8)
B.
Final plasma viral load
10^2
10^3
10^4
10^5
10^6
10^7
p = 0.02
r = −0.81
10^{-3}
10^{-2}
10^{-1}
SHIV–dependent CD8 Prol. (ω_8)
C.
SHIV–dependent CD8 Prol. (ω_8)
10^{-1}
10^{-2}
10^{-3}
p = 0.03
Control
Transplant
D.
Days to rebound (Δ_t)
3
6
9
12
15
18
21
p = 0.01
Control
Transplant

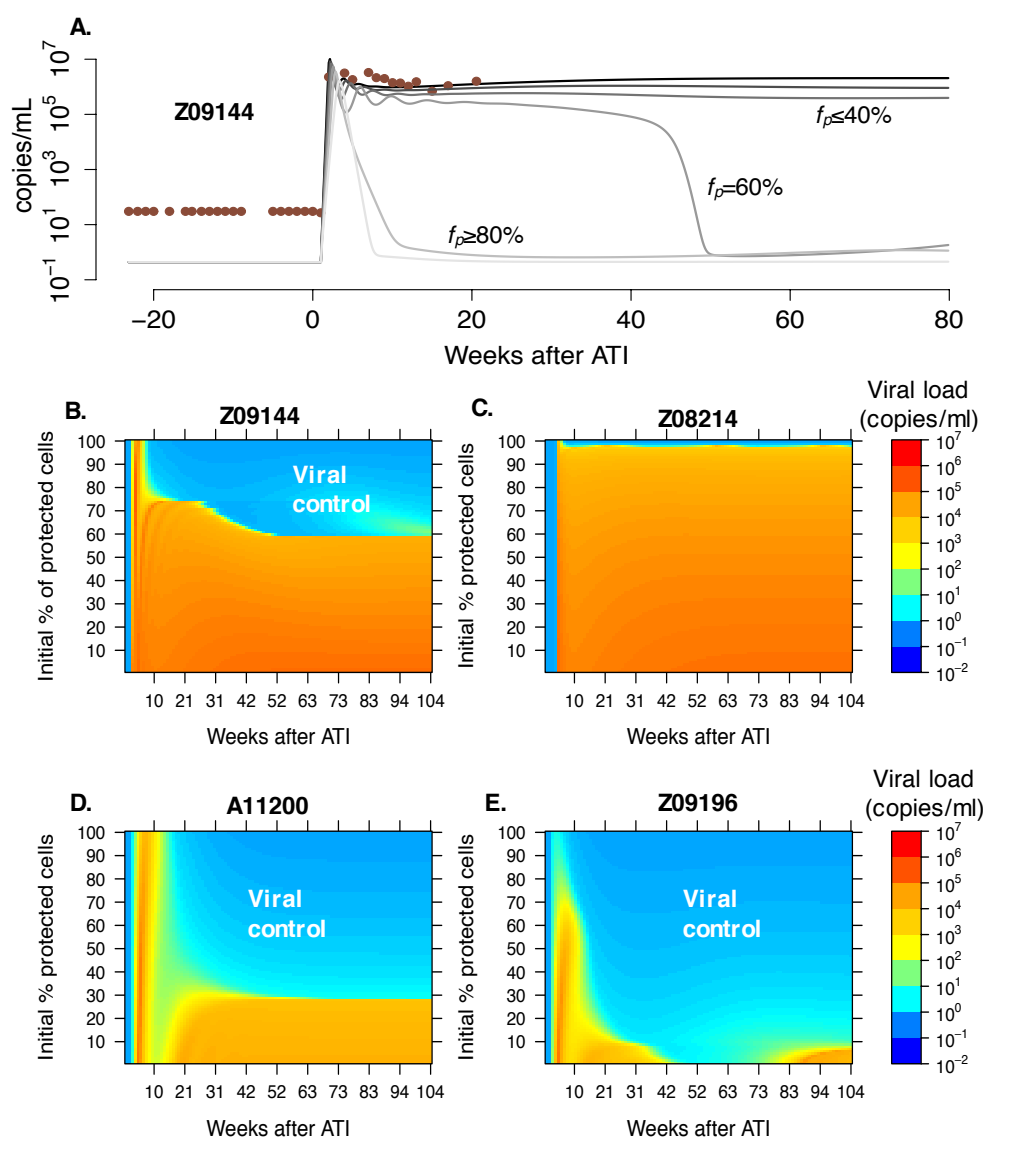
A.
Z09144
copies/mL
10^{-1} 10^{1} 10^{3} 10^{5} 10^{7}
f_p≤40%
f_p=60%
f_p≥80%
−20 0 20 40 60 80
Weeks after ATI
B.
Z09144
Viral control
Initial % of protected cells
10 21 31 42 52 63 73 83 94 104
Weeks after ATI
C.
Z08214
Initial % protected cells
Weeks after ATI
Viral load (copies/ml)
10^{7} 10^{6} 10^{5} 10^{4} 10^{3} 10^{2} 10^{1} 10^{0} 10^{-1} 10^{-2}
D.
A11200
Viral control
Initial % protected cells
Weeks after ATI
E.
Z09196
Viral control
Initial % protected cells
Weeks after ATI
Viral load (copies/ml)

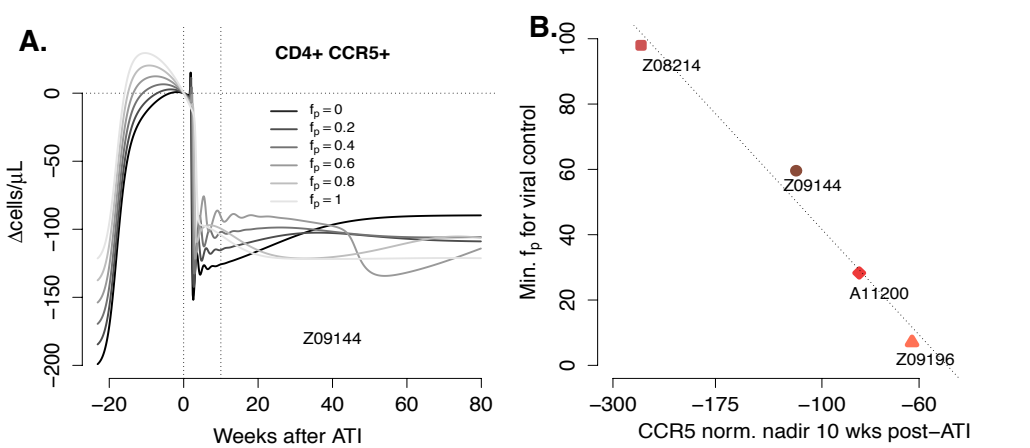
A.
CD4+ CCR5+
$f_p = 0$
$f_p = 0.2$
$f_p = 0.4$
$f_p = 0.6$
$f_p = 0.8$
$f_p = 1$
Z09144
Δcells/μL
0
−50
−100
−150
−200
−20
0
20
40
60
80
Weeks after ATI
B.
Min. f_p for viral control
0
20
40
60
80
100
Z08214
Z09144
A11200
Z09196
−300
−175
−100
−60
CCR5 norm. nadir 10 wks post−ATI